Macromolecules
A R T I C L E

Enhancing the Potential of Block Copolymer Lithography with Polymer Self-Consistent Field Theory Simulations

Rafal A. Mickiewicz,[†,‡] Joel K. W. Yang,[§,||] Adam F. Hannon,[†] Yeon-Sik Jung,[†,⊥] Alfredo Alexander-Katz,[†] Karl K. Berggren,[§] and Caroline A. Ross*[,†]

[†]*Department of Materials Science and Engineering and* [§]*Department of Electrical Engineering and Computer Science, Massachusetts Institute of Technology 77 Massachusetts Avenue Cambridge, Massachusetts 02139.* [‡]*Current address: Fraunhofer Center for Sustainable Energy Systems, 25 First St., Cambridge, MA.* [||]*Current address: Institute of Materials Research and Engineering, 3 Research Link, Singapore 117602.* [⊥]*Current address: Department of Materials Science and Engineering, Korea Advanced Institute of Science and Technology (KAIST), Korea*

ABSTRACT: Self-consistent field theory methodology is used to explore the graphoepitaxy of spherical-morphology block copolymers templated by an array of posts, as well as to predict the formation of aperiodic templated structures, giving an excellent agreement with experimental results. Simulations in two and three dimensions were performed on model hexagonal lattices of posts with spacing, L_{post} that was varied in the range $L_{post} = 1.7L_0$ to $3.9L_0$, where L_0 is the equilibrium period of the block copolymer. The effects of changing the diameter of the posts and the volume fraction of the block copolymer were investigated, and the formation of a structure with designed aperiodicities was successfully modeled.

Introduction

The use of block copolymer (BCP) thin films to define nanoscale patterns for high resolution lithography has been expanding recently thanks to the many advantages afforded by these materials, such as self-assembly, tunability of the pattern geometry and dimensions, and low cost.[1-15] Specifically, block copolymers can assemble into a variety of periodic structures with dimensions of ~5-10 nm and above, providing higher resolution than is possible from existing optical lithography methods, in a low cost, large area process. The period of the BCP structures can be controlled by the degree of polymerization of the block copolymer chains, and the geometry is determined by the volume fraction of the component blocks.[16,17] A drawback to the self-assembly process is that the resulting periodic structures are only ordered locally, and have poor long-range order. In order to impose long-range order, a "top-down" patterning process based on, for example, electron-beam lithography has been used to make a chemical or topographical template on which the BCP can register, yielding periodic patterns with long-range order, or aperiodic features such as lines with angles or junctions.[1-15]
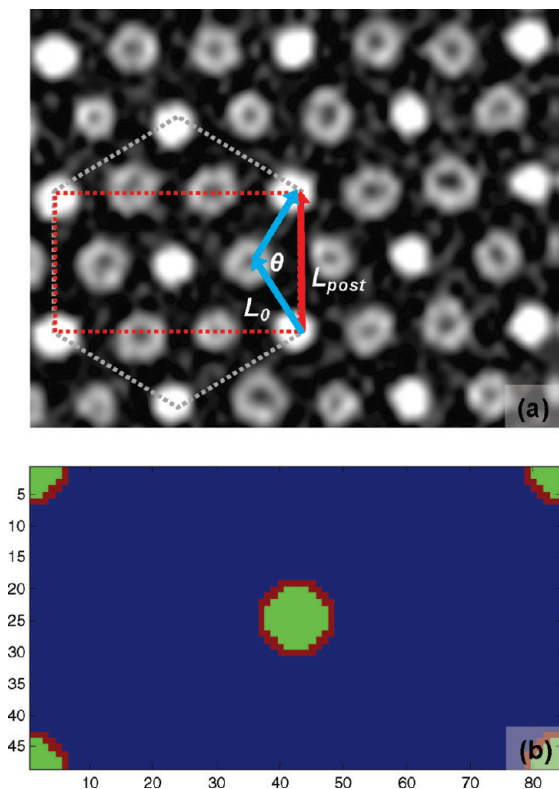
In order to expand the lithographic toolkit, it is desirable to be able to use the limited set of structures available from diblock copolymers (spheres, cylinders, and lamellae) to form arbitrary shapes and patterns, by providing a template of suitable geometry. Experimentally, this is challenging due to the large number of parameters that could be varied. On the other hand, a large set of parameters can be quickly and efficiently explored by using theoretical simulation methods. Recently, self-consistent field theoretic (SCFT) methods have been developed to efficiently compute the equilibrium structures of block copolymers without "a priori" knowledge of the stable morphology.[18-20] In all these approaches, one is interested in finding the minimum of the *mean-field* free energy functional that depends on the local polymer composition. In particular, Matsen approached this problem by screening, in reciprocal space, all the possible space groups available, and finding which one had the lowest free energy.[18] Fredrickson and co-workers subsequently devised a real-space method, in which the system starts in a random configuration and is evolved toward the configuration that minimizes the aforementioned mean-field free energy.[19,20] Fredrickson's approach has been successful in finding the equilibrium morphologies of block copolymers without any structural input. Using this method it has been possible to study the phase behavior of diblock and triblock copolymers,[19,21] nanoparticle–copolymer blends,[22] and confined self-assembly.[23-26] More recently, de Pablo and co-workers have put forward a method to perform the field theoretic simulations, the so-called theoretically informed coarse grain simulations, by evaluating the partition function of the polymers explicitly using Monte Carlo techniques. This has been successfully applied to study the self-assembly of block copolymers above chemically patterned surfaces, as well as nanocomposites.[2,27,28] This method does not rely on the mean-field approximation and is equivalent to sampling the full energy functional, and in principle corresponds to the field-theoretic simulation (FTS) method developed by Fredrickson and co-workers.[19,29,30]

Experimental System and Simulation Methods

In this article, we describe the use of the SCFT methodology to explore the graphoepitaxy of spherical-morphology block copolymers templated by an array of posts, as well as to predict the formation of aperiodic templated structures, and we demonstrate an excellent agreement between the model and experimental results. The experiment[3] used a template consisting of a hexagonal lattice of nanoscale topographical patterns (posts) with period L_{post}, diameter ~15 nm and height 30 nm, to control the self-assembly of a sphere-forming polystyrene-*b*-polydimethylsiloxane (PS-*b*-PDMS) diblock copolymer with a PDMS volume
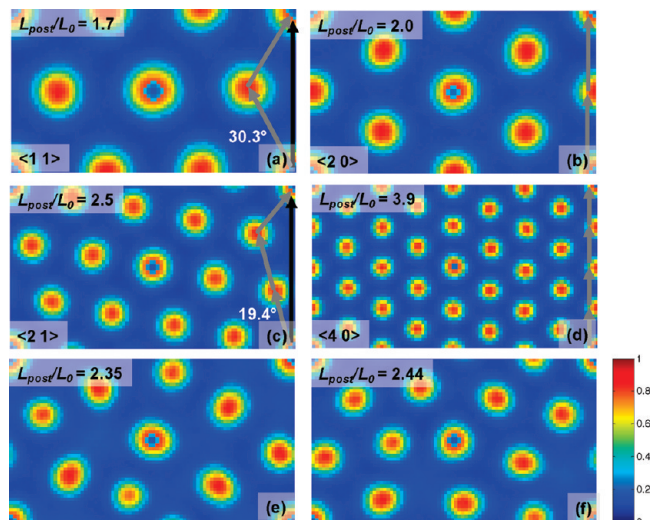
*Corresponding author.

Figure 2. Selected simulation results showing the orientation of the BCP lattice relative to the post lattice, which is dictated by the spacing of the posts, L_{post}, relative to the equilibrium BCP spacing, L_0. $L_{post}/L_0 =$ (a) 1.7, (b) 2.0, (c) 2.5, (d) 3.9, (e) 2.35, and (f) 2.44. The color scale represents the relative density distribution of the minority block of the BCP. Red indicates 100% density of the minority block, while blue represents 0%. The posts are light blue regions inside some of the minority block microdomains: (a–d) ordered lattices; (e, f) disordered lattices. (d) Shows an area four times larger than (a-c) and (e,f).

Figure 1. (a) SEM image of a templated array of PDMS spheres from a PS−PDMS block copolymer. The bright circles are the HSQ posts and the gray circles are the oxidized PDMS microdomains of the BCP. The post lattice and BCP lattice basis vectors are overlaid onto the image, and enclose an angle of 120° in the $\langle 1\ 1 \rangle$ orientation depicted in the image. (b) Layout of the post template for the simulations. The green areas represent the HSQ posts and the red area represents the PDMS brush. The size of the posts was varied depending on the scaled dimension of the simulation box, in order to be on the order of the size of a spherical domain. The rectangular section corresponds to a portion of the hexagonal post lattice depicted by the red dotted lines in part a.

fraction $f_{PDMS} = 0.165$ and an equilibrium period of $L_0 = 40$ nm. The posts were made on an oxidized silicon wafer from a hydrogen silsesquioxane (HSQ) resist using electron-beam lithography,[3,31] and the posts and wafer were subsequently treated with a PDMS brush layer to make them attractive to the PDMS block of the copolymer. The topographical template was then coated with a film of PS-*b*-PDMS which was annealed at 200 °C to promote microphase segregation, forming a monolayer of PDMS spheres in a PS matrix.

The PDMS spheres self-assembled into a well-ordered close packed array in which the posts "substituted" for PDMS spheres, i.e., each post occupied one lattice site in the sphere array. The arrangement of spheres was determined by the ratio L_{post}/L_0, which varied from 1.5 to 4.5 in the experiment. In most cases, a close-packed lattice of spheres with few defects was formed. If the post lattice was incommensurate with the sphere lattice, the period L of the sphere lattice was strained with respect to L_0. We found that for all values of L_{post}, L satisfies the relation $L_{post}/L = (i^2 + j^2 + ij)^{1/2}$, where i and j are integers. We designate the sphere lattice $\langle i\ j \rangle$, as shown in Figure 1a, which illustrates a $\langle 1\ 1 \rangle$ lattice. The angle between the basis vectors of the sphere lattice and of the post lattice is given by $\theta = \cos^{-1}((2i + j)/(2(i^2 + j^2 + ij)))^{1/2}$. The observed lattices $\langle i\ j \rangle$ that formed as a function of L_{post} were consistent with a model that minimized the strain energy in the sphere lattice.

SCFT was used to model these experimental results, and we show that SCFT modeling can also be used to predict self-assembly on templates of lower symmetry. In SCFT, the diblock copolymers are considered to be Gaussian chains composed of two blocks, A and B, covalently bonded at the junction point. The chemical incompatibility between the different blocks is characterized through the Flory−Huggins interaction parameter χ. The melt is assumed to be incompressible. By using standard mathematical techniques, the particle based partition function is transformed to a field theory that only depends on a pressure field w_+ and an exchange potential field $w\text{-}$[19,20] (see Supporting Information, SI). The topographic posts are treated as regions where polymers cannot penetrate by adding an additional spatially varying local external field[24] with a fixed field value of $w_+ = -20$. An external exchange potential field $w\text{-} = 10$ was also added at the surface of the posts to model the preferential wetting of the posts by the PDMS blocks. This external potential simulated the PDMS brush, and its magnitude was determined from the average exchange potential in the center of PDMS lamellae modeled with the same χN, where N is the number of statistical segments in the polymer chain.
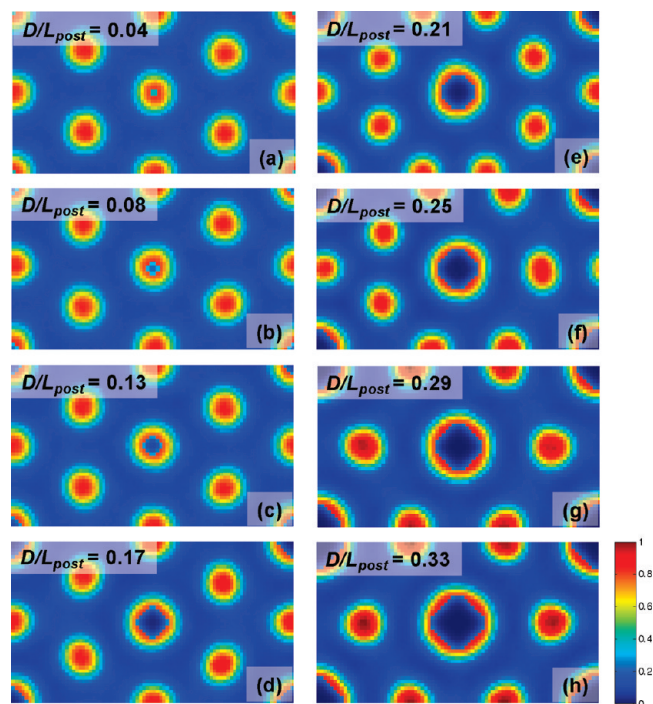
Results and Discussion

We first discuss the results of a two-dimensional model. A unit cell of the hexagonal post lattice (Figure 1b) was represented by an 84 × 48 pixel rectangular cell with periodic boundary conditions. The polymer had a minority (PDMS) volume fraction $f = 0.25$ and $\chi N = 18$. This model volume fraction exceeds that of the experimental polymer, but was selected so that the spheres could be represented as vertical cylinders in the 2D model. The 2D volume fraction of the simulation corresponds to the observed area fraction (~0.23) of the spheres in the experiment, seen in Figure 1a.

Figure 2 shows the results of selected simulations where the ratio of post lattice spacing to the equilibrium spacing of the polymer, L_{post}/L_0, was varied. For most values of L_{post}/L_0, an ordered arrangement of BCP microdomains formed, in which the basis vectors of the BCP lattice make an angle θ with the basis vectors of the post lattice. Comparison with experiment shows an excellent match between the SCFT model and the analytical
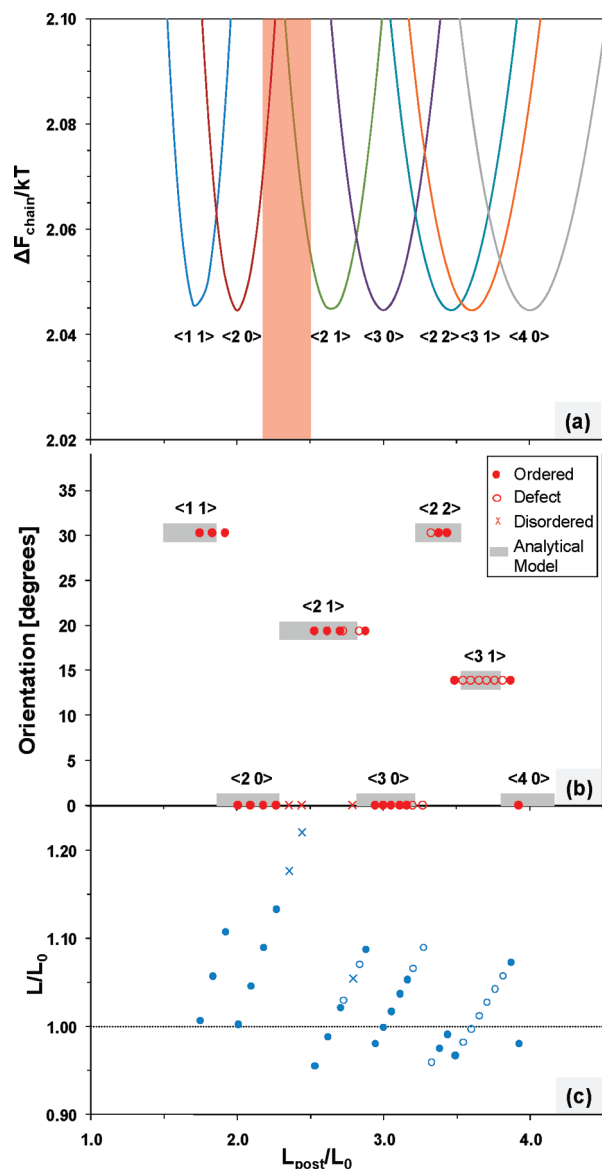
Figure 3. (a) Predictions of an analytical model showing the free energy per polymer chain vs L_{post}/L_0 for different lattice types.[3] (b) Orientation of the BCP lattice relative to the underlying post lattice for the analytical model (gray bars) and for the results of the SCFT model. The points marked by "×" indicate disordered BCP lattices such as those in Figure 2e,f and are shown at $\theta = 0°$. (c) Lattice parameter of the microdomain lattice normalized to the equilibrium spacing, from the SCFT model. The data for the disordered lattices represent average spacings between microdomains.
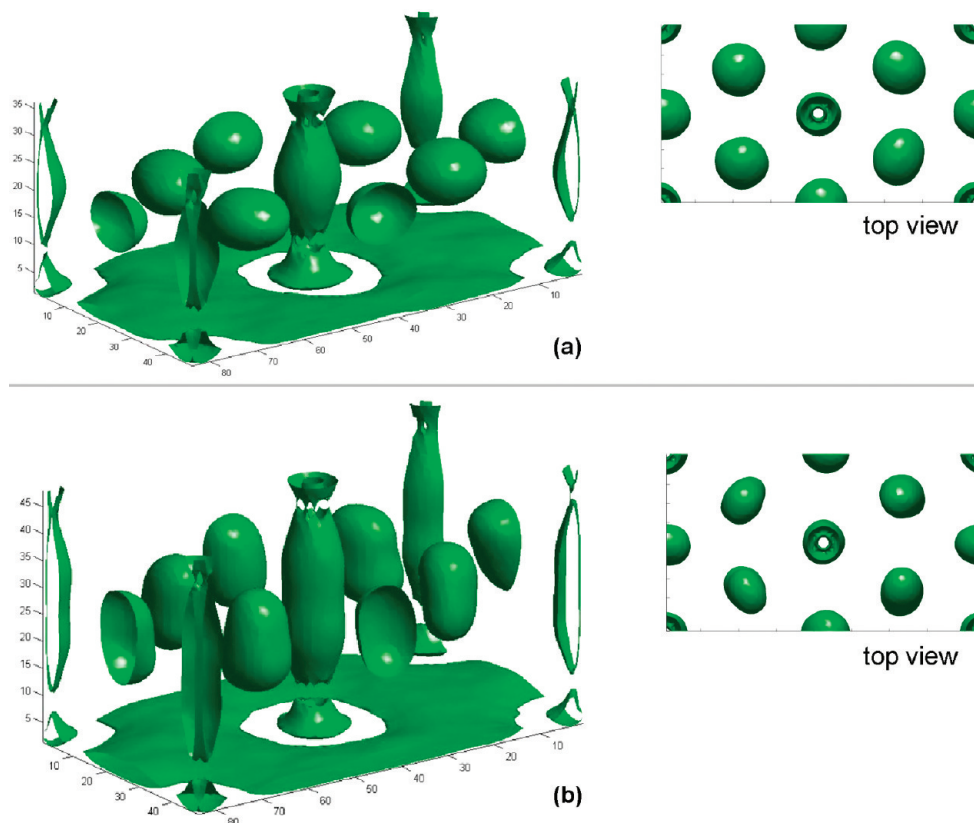

Figure 4. Effect of increasing lattice post diameter D on the orientation of the BCP lattice for $L_{post}/L_0 = 2.0$. (a−h) $D/L_{post} = 0.04$, 0.08, 0.13, 0.17, 0.21, 0.25, 0.29, 0.33 respectively. The $\langle 2\,0 \rangle$ lattice forms in (a−d), but larger post sizes lead to a higher coordination number in (e) and (f), and a $\langle 1\,1 \rangle$ lattice for (g) and (h).
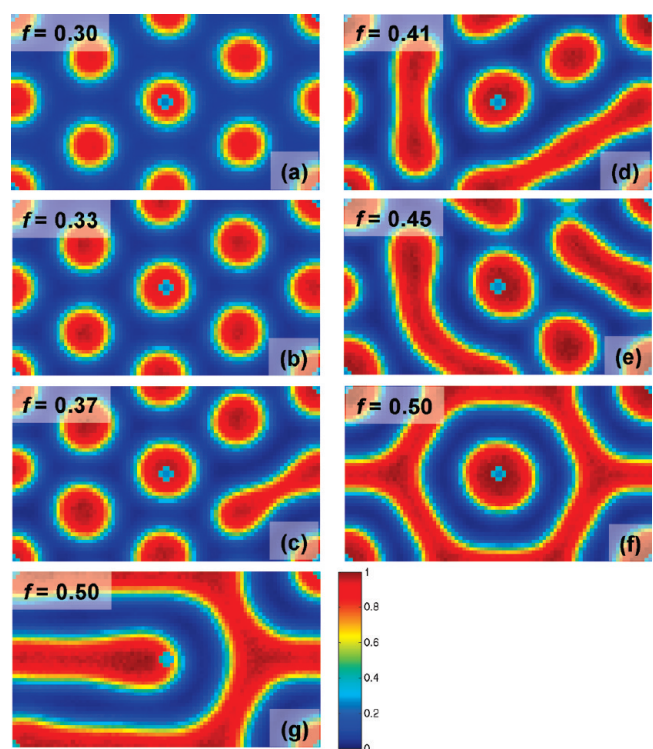
Figure 5. Effect of changing volume fraction f on the microphase separated structure for lattice with $L_{post}/L_0 = 2.18$: (a−f) $f = 0.30$, 0.33, 0.37, 0.41, 0.45, 0.50, respectively. Increasing volume fraction drives the systems from a $<2\ 0>$ lattice (a, b) to a structure with microdomains that are elongated in plane (d, e), and finally to a lamellar network (f). In (g), the exchange potential $w_- = 5$, reducing the attraction of the minority block to the guiding post lattice.

model (summarized in the SI), which itself agrees with the experimental results.[3] Figure 3a shows the predicted lattice type $\langle i\,j \rangle$ from the analytical free-energy model as a function of L_{post}/L_0, and Figure 3b shows the corresponding orientation angle θ indicated with gray bars. Superposed in Figure 3b are the values of θ from the SCFT model. In many of the simulations (indicated with solid symbols) a defect-free lattice formed of the type $\langle i\,j \rangle$ and orientation θ expected from the analytical model. We also observed the formation of lattices with defects (open circles) or disordered structures (crosses). We define a defective lattice as one in which an underlying orientation of the lattice exists, despite the presence of defects, while a disordered lattice has no dominant orientation. (The data points for the disordered structures are marked on the horizontal axis since the angle θ is not well-defined.) Multiple simulations performed at a particular L_{post}/L_0, but with different initial conditions, gave similar results for lattice orientation,

Figure 6. Constant density surfaces of the 3D simulation with $f = 0.25$ and $L_{post}/L_0 = 2.0$: (a) $z = 0.75 L_{post}$, 500 000 iterations; (b) $z = 1.0 L_{post}$, 320 000 iterations. In both cases the inset at right shows the top view, excluding the brush layers. The contours show the locations where the volume fraction is 0.5, representing the intermaterial dividing surface between the two blocks. In both figures, the minority block wets the posts and the bottom surface, and additionally forms distorted spherical microdomains, flattened in the z-direction (a) and elongated in the z-direction (b), around the posts in a $\langle 2\,0 \rangle$ lattice.

though with differences in the details of the defects present (see SI for the case $L_{post}/L_0 = 3.61$).

Because of the importance of commensurability in the templating process, it is instructive to calculate the strain in the templated sphere lattice predicted by the computational model. Figure 3c shows the period of the array normalized to the equilibrium period, L/L_0, as a function of L_{post}/L_0. The model reveals significant strain in the templated array, up to $\pm 10\%$, before the lattice orientation changes. Experimental work on lamellar BCP systems templated onto chemically patterned surfaces showed similar results, where the native BCP lattice spacing could be strained up to $\pm 10\%$ before significant defect formation was observed.[7,32] The results here suggest that tensile strain is more readily accommodated than compressive strain, as seen experimentally in a lamellar block copolymer templated between flat plates[33] and a spherical block copolymer templated on a patterned substrate.[34] In certain ranges of L_{post}/L_0 where the strain energy of the possible ordered lattices is relatively high, structures with many defects are observed. An example is $L_{post}/L_0 \sim 2.4$, where the competing lattices are $\langle 2\,0 \rangle$ (strain-free when $L_{post}/L_0 = 2.0$) and $\langle 2\,1 \rangle$ (strain-free when $L_{post}/L_0 = \sqrt{7} = 2.65$). At $L_{post}/L_0 \sim 2.4$, formation of these lattices would require tensile strain of 20% for $\langle 2\,0 \rangle$ and compressive strain of 14% for $\langle 2\,1 \rangle$. Figure 2(e,f) shows examples of disordered lattices that form around $L_{post}/L_0 \sim 2.4$. Experimentally, at these post spacings, mixtures of different lattices are observed across the sample (e.g., $\langle 2\,0 \rangle$, $\langle 2\,1 \rangle$, and $\langle 3\,1 \rangle$ coexisting), but the small size of the computational cell and the periodic boundary conditions prevent this from occurring in the simulation, making the formation of disordered structures more likely as the calculation becomes trapped in metastable configurations.

Having established the ability of the SCFT simulations to reproduce the observations of templating a BCP lattice, we now discuss the effects of other system parameters, namely the post diameter and BCP volume fraction (Figure 4 and Figure 5, respectively). In the former case, simulations were carried out at $L_{post}/L_0 = 2$, at which the $\langle 2\,0 \rangle$ lattice was expected to form. The ratio of post diameter, D, to L_{post} varied from 0.04 to 0.33. The $\langle 2\,0 \rangle$ lattice forms robustly up to $D/L_{post} = 0.17$, accompanied by a distortion of the microdomains. There is an abrupt change for $D/L_{post} = 0.21-0.25$, where the coordination of the microdomains around the posts rises above six, and at $D/L_{post} = 0.29$ the system transitions to a $\langle 1\,1 \rangle$ lattice orientation as the space between the posts becomes too small for microdomains to form between the posts.

The effect of varying the volume fraction f in the range 0.30−0.50 is given in Figure 5 for $L_{post}/L_0 = 2.18$ and $D/L_{post} = 0.08$. Increasing f leads first to an increase in the diameter of the minority microdomains, then a transition into elongated domains with poor order. At $f = 0.5$ (Figure 5f), the system exhibits a lamellar morphology. This was expected to form a structure consisting of lamellae parallel to one of three symmetry axes: horizontally from left to right, or at $\pm 60°$ to the horizontal direction. However, the model instead formed a structure in which the posts are surrounded by the minority block, and an interconnected lamellar structure forms between the posts with sections parallel to the three symmetry axes. This appears to be a metastable structure that represents the system "sampling" the three possible lamellar orientations. It occurs as a result of the strong attraction of the minority block to the posts, which leads to a layer of the majority block surrounding the posts and generates the symmetrical honeycomb structure seen in Figure 5f. By making the
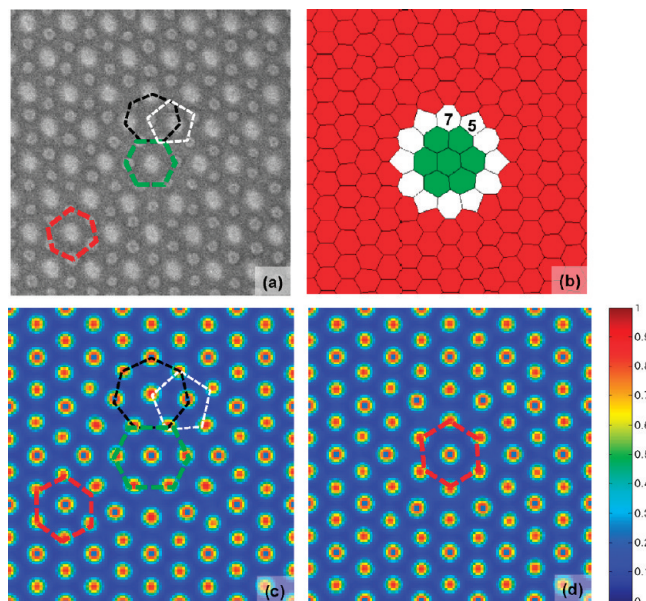
Figure 7. Comparison of experimental and simulated results on a post lattice with a deliberate defect. (a) SEM image of posts (bright) and microdomains (gray), with lattice orientation color coded according to the scheme in part b, showing a Voronoi figure based on the SEM image. The region of the image shaded red shows a $\langle 1\,1 \rangle$ lattice, while the region shaded green shows a $\langle 2\,0 \rangle$ lattice. The white domains have 7-fold or 5-fold coordination, and are depicted in (a) as black and white dashed regions, respectively. (c) Simulation showing the same result as the experiment. The microdomains are color-coded as in part a to show their coordination. (d) Change in the post arrangement (see text for details) leads to a $\langle 1\,1 \rangle$ lattice across the entire sample.

potential field around the posts less attractive, the simulation results in the expected lamellar orientation, albeit with a defect (Figure 5g). By reducing the symmetry of the post lattice from 6-fold to 2-fold, an arrangement of parallel lamellae registered on the posts can be obtained from the model for a range of post spacings at $f = 0.5$.[35]

In order to examine the 3D structure of the microphase-separated block copolymer, 3D simulations were performed with a volume fraction of $f = 0.25$ at $L_{post}/L_0 = 2.0$. The 84×48 pixel rectangular cell lattice had a height in the z-direction of either 36 or 48 pixels, corresponding to a thickness of 0.75 and 1.0 times L_{post}, respectively. These thicknesses are within the commensurability range in width observed for the formation of a single row of spherical domains of a block copolymer in a narrow topographical channel.[36] The boundary condition at the bottom surface of the simulation box was modeled in the same fashion as the posts, i.e., attractive to the minority block. This condition is consistent with the experiment, in which PDMS, the minority component, wets the PDMS-brushed substrate and posts. The top surface is neutral. As seen in Figure 6, the minority block wets the posts and the bottom surface, and forms distorted spherical microdomains between the posts in locations corresponding to the $\langle 2\,0 \rangle$ lattice. The elongation of the spheres in the z-direction in the 48 pixel thick simulation relative to the 36 pixel thick simulation is a response to the modeled film thickness being greater than the thickness of one monolayer of spheres plus the brush layer. Overall, the 3D model gives a good general agreement with the structure believed to form in the experiment, reproducing the 6-fold symmetry of the microdomains, the $\langle 2\,0 \rangle$ lattice, and the wetting behavior.

We finally describe the effects of templating around an intentional defect in a post lattice with $L_{post}/L_0 = \sqrt{3}$. To create the defect in this lattice, six posts surrounding an arbitrarily chosen center post were shifted away from the center post so that the

distance between them and the center post was increased by a factor of 1.15. This gives a spacing of $2L_0$ between these six posts and the center, Figure 7a. As expected, a $\langle 1\,1 \rangle$ sphere array formed in the bulk of the template, but at the defect, a $\langle 2\,0 \rangle$ lattice was formed, oriented at 30° to the surrounding $\langle 1\,1 \rangle$ lattice. Where the two lattices meet, a ring of 5-fold and 7-fold coordinated spheres formed (Figure 7b). A 2D simulation was performed on a 114×110 pixel unit cell containing this template structure. The results are shown in Figure 7(c), which gives an excellent agreement with the experimental result. Figure 7(d) shows the effect of a horizontal shift of the central post by $\sim 0.08 L_0$. This resulted in an aligned defect-free $\langle 1\,1 \rangle$ lattice, underscoring the sensitivity of the BCP self-assembly to relatively small changes in template spacing.

Conclusion

In summary, polymer SCFT simulations have been successfully used to model the structures formed by the graphoepitaxy of a spherical-morphology block copolymer on an array of lithographically defined posts. These simulations are capable of accurately reproducing the effects of commensurability as observed experimentally. SCFT provides the means to explore the effects of parameters that may be inconvenient to test experimentally, to visualize the 3D structure of the microdomains, and to predict morphologies resulting from nonperiodic templates. As a result, SCFT simulations can efficiently validate different template structures, enabling the rational design of templates for BCP lithography.

Supporting Information Available: Text giving model description, anaylsis of the model, and discussion of the simulation and figures showing the external field profile and simulation results. This material is available free of charge via the Internet at http://pubs.acs.org.

References and Notes

(1) Cheng, J. Y.; Ross, C. A.; Thomas, E. L.; Smith, H. I.; Vancso, G. J. *Adv. Mater.* **2003**, *15*, 1599–1602.
(2) Stoykovich, M. P.; Muller, M.; Kim, S. O.; Solak, H. H.; Edwards, E. W.; de Pablo, J. J.; Nealey, P. F. *Science* **2005**, *308*, 1442–1446.
(3) Bita, I.; Yang, J. K. W.; Jung, Y. S.; Ross, C. A.; Thomas, E. L.; Berggren, K. K. *Science* **2008**, *321*, 939–943.
(4) Cheng, J. Y.; Rettner, C. T.; Sanders, D. P.; Kim, H. C.; Hinsberg, W. D. *Adv. Mater.* **2008**, *20*, 3155–3158.
(5) Ruiz, R.; Kang, H. M.; Detcheverry, F. A.; Dobisz, E.; Kercher, D. S.; Albrecht, T. R.; de Pablo, J. J.; Nealey, P. F. *Science* **2008**, *321*, 936–939.
(6) Park, S.; Lee, D. H.; Xu, J.; Kim, B.; Hong, S. W.; Jeong, U.; Xu, T.; Russell, T. P. *Science* **2009**, *323*, 1030–1033.
(7) Kim, S. O.; Solak, H. H.; Stoykovich, M. P.; Ferrier, N. J.; de Pablo, J. J.; Nealey, P. F. *Nature* **2003**, *424*, 411–414.
(8) Wilmes, G. M.; Durkee, D. A.; Balsara, N. P.; Liddle, J. A. *Macromolecules* **2006**, *39*, 2435–2437.
(9) Segalman, R. A.; Hexemer, A.; Kramer, E. J. *Phys. Rev. Lett.* **2003**, *91*, 196101.
(10) Segalman, R. A.; Yokoyama, H.; Kramer, E. J. *Adv. Mater.* **2001**, *13*, 1152–1155.
(11) Stoykovich, M. P.; Kang, H.; Daoulas, K. C.; Liu, G.; Liu, C. C.; de Pablo, J. J.; Mueller, M.; Nealey, P. F. *ACS Nano* **2007**, *1*, 168–175.
(12) Sundrani, D.; Darling, S. B.; Sibener, S. J. *Nano Lett.* **2004**, *4*, 273–276.

(13) Black, C. T.; Bezencenet, O. *IEEE Trans. Nanotechnol.* **2004**, *3*, 412–415.

(14) Cheng, J. Y.; Mayes, A. M.; Ross, C. A. *Nat. Mater.* **2004**, *3*, 823–828.

(15) Park, S. M.; Craig, G. S. W.; La, Y. H.; Solak, H. H.; Nealey, P. F. *Macromolecules* **2007**, *40*, 5084–5094.

(16) Bates, F. S.; Fredrickson, G. H. *Phys. Today* **1999**, *52*, 32–38.

(17) Bates, F. S.; Fredrickson, G. H. *Annu. Rev. Phys. Chem.* **1990**, *41*, 525–557.

(18) Matsen, M. W.; Schick, M. *Phys. Rev. Lett.* **1994**, *72*, 2660–2663.

(19) Fredrickson, G. H.; Ganesan, V.; Drolet, F. *Macromolecules* **2002**, *35*, 16–39.

(20) Fredrickson, G. H. *The Equilibrium Theory of Inhomogeneous Polymers*; Oxford University Press: New York, 2006; Vol. *134*.

(21) Cochran, E. W.; Garcia-Cervera, C. J.; Fredrickson, G. H. *Macromolecules* **2006**, *39*, 2449–2451.

(22) Sides, S. W.; Kim, B. J.; Kramer, E. J.; Fredrickson, G. H. *Phys. Rev. Lett.* **2006**, 96.

(23) Wu, Y. Y.; Cheng, G. S.; Katsov, K.; Sides, S. W.; Wang, J. F.; Tang, J.; Fredrickson, G. H.; Moskovits, M.; Stucky, G. D. *Nat. Mater.* **2004**, *3*, 816–822.

(24) Bosse, A. W.; Garcia-Cervera, C. J.; Fredrickson, G. H. *Macromolecules* **2007**, *40*, 9570–9581.

(25) Stein, G. E.; Cochran, E. W.; Katsov, K.; Fredrickson, G. H.; Kramer, E. J.; Li, X.; Wang, J. *Phys. Rev. Lett.* **2007**, 98.

(26) Hur, S. M.; Garcia-Cervera, C. J.; Kramer, E. J.; Fredrickson, G. H. *Macromolecules* **2009**, *42*, 5861–5872.

(27) Pike, D. Q.; Detcheverry, F. A.; Muller, M.; de Pablo, J. J. *J. Chem. Phys.* **2009**, 131.

(28) Detcheverry, F. A.; Kang, H. M.; Daoulas, K. C.; Muller, M.; Nealey, P. F.; de Pablo, J. J. *Macromolecules* **2008**, *41*, 4989–5001.

(29) Alexander-Katz, A.; Fredrickson, G. H. *Macromolecules* **2007**, *40*, 4075–4087.

(30) Alexander-Katz, A.; Moreira, A. G.; Fredrickson, G. H. *J. Chem. Phys.* **2003**, *118*, 9030–9036.

(31) Yang, J. K. W.; Berggren, K. K. *J. Vac. Sci. Technol. B* **2007**, *25*, 2025–2029.

(32) Edwards, E. W.; Montague, M. F.; Solak, H. H.; Hawker, C. J.; Nealey, P. F. *Adv. Mater.* **2004**, *16*, 1315–1319.

(33) Lambooy, P.; Russell, T. P.; Kellogg, G. J.; Mayes, A. M.; Gallagher, P. D.; Satija, S. K. *Phys. Rev. Lett.* **1994**, *72*, 2899–2902.

(34) Xiao, S. G.; Yang, X. M.; Park, S. J.; Weller, D.; Russell, T. P. *Adv. Mater.* **2009**, *21*, 2516-+.

(35) Yang, J. K. W.; Jung, Y. S.; Chang, J. B.; Mickiewicz, R. A.; Alexander-Katz, A.; Ross, C. A.; Berggren, K. K. *Nature Nanotechnol.* **2010**, *5*, 256–260.

(36) Cheng, J. Y.; Zhang, F.; Chuang, V. P.; Mayes, A. M.; Ross, C. A. *Nano Lett.* **2006**, *6*, 2099–2103.